Multi-wavelength High Efficiency Laser System for Lidar Applications

Christina C. C. Willis*[a], Charles Culpepper[a], Ralph Burnham[a]
[a]Fibertek, Inc., 13605 Dulles Technology Drive, Herndon, VA, USA 20171

ABSTRACT

Motivated by the growing need for more efficient, high output power laser transmitters, we demonstrate a multi-wavelength laser system for lidar-based applications. The demonstration is performed in two stages, proving energy scaling and nonlinear conversion independently for later combination. Energy scaling is demonstrated using a 1064 nm MOPA system which employs two novel ceramic Nd:YAG slab amplifiers, the structure of which is designed to improve the amplifier's thermal performance and energy extraction via three progressive doping stages. This structure improved the extraction efficiency by 19% over previous single-stage dopant designs. A maximum energy of 34 mJ was produced at 500 Hz with a 10.8 ns pulse duration. High efficiency non-linear conversion from 1064 nm to 452 nm is demonstrated using a KTP ring OPO with a BBO intra-cavity doubler pumped with 50 Hz, 16 ns 1064 nm pulses. The OPO generates 1571 nm signal which is frequency doubled to 756 nm by the BBO. Output 786 nm pulses are mixed with the 1064 nm pump pulses to generate 452 nm. A conversion efficiency of 17.1% was achieved, generating 3 mJ of 452 nm pulses of 7.8 ns duration. Pump power was limited by intra-cavity damage thresholds, and in future experiments we anticipate >20% conversion efficiency.

Keywords: Blue, Lidar, HSRL, Optical Parametric Oscillator, Sum-Frequency Mixing

1. BACKGROUND & MOTIVATION FOR HIGH POWER, MULTILINE LIDAR SYSTEM

The use of lidar in a wide variety of scientific fields yields a wealth of valuable data, and scaling to higher powers and expanding to multiple wavelengths serves to expand the types and quality of data that can be acquired. According to this growing need for higher performance, Fibertek has developed a new generation of solid-state lasers capable of meeting the requirements for higher efficiency and scalability to output powers of >100 W. Proof of concept is demonstrated for a system with high power, multiline single-frequency output (1064 nm, 532 nm, and 355 nm), and narrow linewidth output in the blue-green region, selectable between 450 and 490 nm.

The availability of wavelengths in the blue region would allow such the transmitter to be used for measurements of deep subsurface ocean scattering, providing unprecedented capability for direct depth-resolved measurements of the ocean ecosystem. Blue light between 450 and 470 nm has a diffuse attenuation coefficient (k_d) that is ~1/5 that of 532 nm light [1]. The additional wavelength channel in the blue will make it possible to quantify the differences in scattering between coastal and mid-ocean type water. In addition to providing measurement of the mixing between these regions, the blue channel would provide direct measurement of depth-resolved scattering from the entire oceanic mixed layer to the thermocline. The ~5:1 ratio of k_d between blue and green light for ocean-type water (Figure 1) also provides firm basis for determination of ocean particulate content on a global scale using a two-color blue-green lidar.

The demonstration of this system is performed with two separate experiments. The first relates to the subject of energy scaling, and the second to efficient non-linear frequency conversion. For the energy scaling portion, and new amplifier slab design was implemented, utilizing incremented doping stages, to enable better extraction efficiency and higher output energies. An extraction efficiency of 24.6% was achieved, which represents a 19% improvement over prior slab designs. The high energy output from this system can be used to generate 532 and 355 nm and tunable blue output via non-linear conversion.

For the non-linear experiments demonstrating blue light generation, an experimental set up was developed to convert 1064 nm into 452 nm light via several non-linear conversion stages, and a 17% optical-to-optical conversion efficiency was obtained. While doubling 946 nm light directly can yield blue light at 473 nm with efficiencies approaching 50% [2], the output is not wavelength tunable and generating high power 946 nm light has its own complications due to a small stimulated emission cross-section and the three-level nature of the transitions. Conversion efficiency as high as 25% to 459 nm using single pass sum-frequency generation has been demonstrated, but required two independently tunable pump sources [3]. A variety of other multi-stage non-linear conversion methods exist for generating blue light,

*cwillis@fibertek.com; phone 1 704 471 7671; fax 1 703 471 5806; Fibertek.com

Lidar Remote Sensing for Environmental Monitoring XV, edited by
Upendra N. Singh, Proc. of SPIE Vol. 9612, 96120I · © 2015 SPIE
CCC code: 0277-786X/15/$18 · doi: 10.1117/12.2191727

but with optical-to-optical conversion efficiencies typically below 10% [4-6]. As such, the demonstrated optical-to-optical conversion efficiency of 17% using only a single pump source, with a tunable blue output, represents a high efficiency method for generating blue light.

Valuable oceanographic data can be acquired with a high power multiline lidar transmitter capable of providing narrow linewidth output in the near IR, green, blue and UV. Such a system will be able to take high spectral resolution lidar (HSRL) measurements in both the atmosphere and water column, as well as measurement of total backscatter. When coupled with a frequency-shift sensitive receiver, application of HSRL to water facilitates both direct measurement of absolute particle scattering cross-sections, and measurement of depth-resolved water temperature and/or salinity. Achieving this capability via the lidar system described here would constitute a significant advance in the study of the atmospheric and oceanic ecosystems.

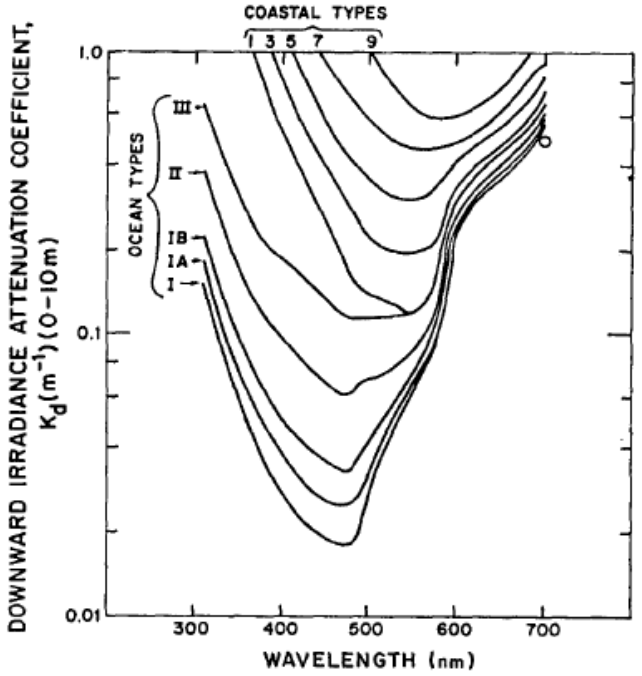

Figure 1: Diffuse attenuation coefficient (k_d) vs. wavelength for coastal and ocean-type waters [1]

2. ENERGY SCALING EXPERIMENTS

In order to demonstrate the system's ability to produce both high power, and high efficiency non-linear optical conversion, the two aspects were tested independently. The first experiment employs a new type of amplifier slab with a design that increases energy extraction by 19% over prior designs.

Energy Scaling Experimental Set Up

To demonstrate energy scalability, a new amplifier slab design is used to increase the extraction efficiency of a 1064 nm MOPA system. While the original (standard) slab design consists of an undoped end cap bonded to a single doped section of uniformly doped Nd:YAG, the new design has three distinct regions of doping concentration: an un-doped endcap, followed two distinct regions of increasing doping concentration. The progressive doping of the new design is crafted to improve the thermal performance of the slab. The new slabs were also made of ceramic instead of crystalline YAG, because doped ceramic YAG is known to have similar thermal properties, relative ease of diffusion bonding, and more homogenous doping distribution.

Modeling of the slabs shows that having a two doped regions, a lower doped section followed by a higher doped section, allows for the same amount of energy absorption as a single, uniformly doped region, but with lower temperature excursions. This effectively spreads the deposited energy in the slab along its length, resulting in a lower peak temperature. The reduced temperature allows for greater gain from the slab as well as better matching to the oscillator wavelength (oscillator slabs are not as strongly pumped, and therefore of lower temperature). The calculated thermal

profiles for the two cases show that multi-layer slab has peak temperature that is almost 50% lower than that of the standard slab (Figure 2).

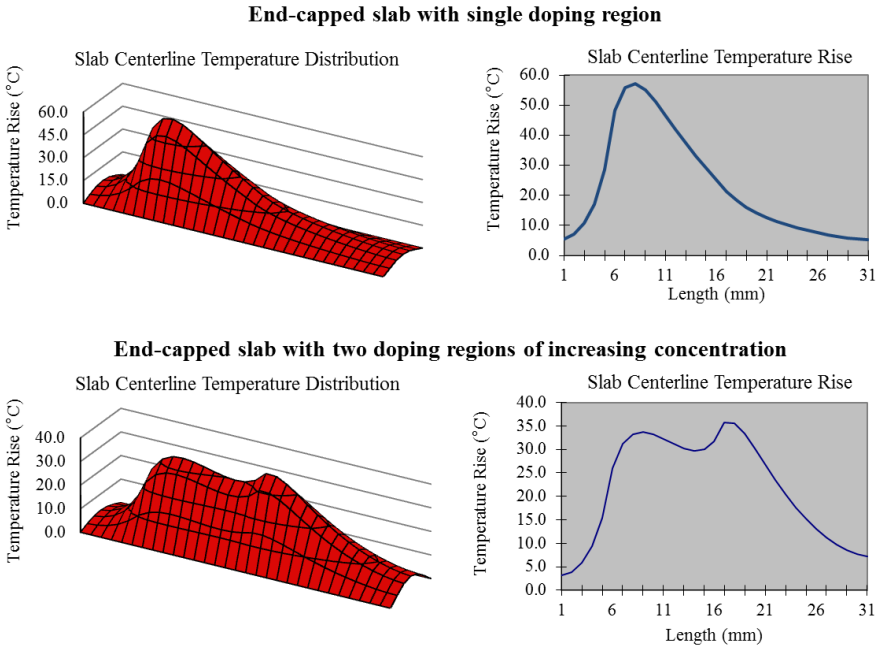

Figure 2: Calculated thermal profiles for single layer slab and multi-layer rods

A ring oscillator using end pumped slabs of standard design was used as the Master Oscillator (MO) for these tests. The MO was seeded by a CW narrow linewidth laser in order to ensure narrow spectral operation, and operated at repetition rate of 500 Hz with up to 14 mJ per pulse. Output from the MO was controlled with a light valve consisting of a λ/2 waveplate and a Thin Film Polarizer (TFP). The light valve gives control over input seed pulse energy while maintaining the input pulse characteristics (pulse width and shape), because it allows the oscillator pump power to be held at a constant level.

Two amplifier set-ups were used; one employing only a single amplifier stage and a second using two amplifier stages (Figure 3). In the single amplifier set up, a single standard slab design was tested in direct comparison to a single stage of the new amplifier design. Once testing was complete, a second amplifier using the novel design was placed after the first stage allowing for the performance of two slabs of the new design to be characterized.

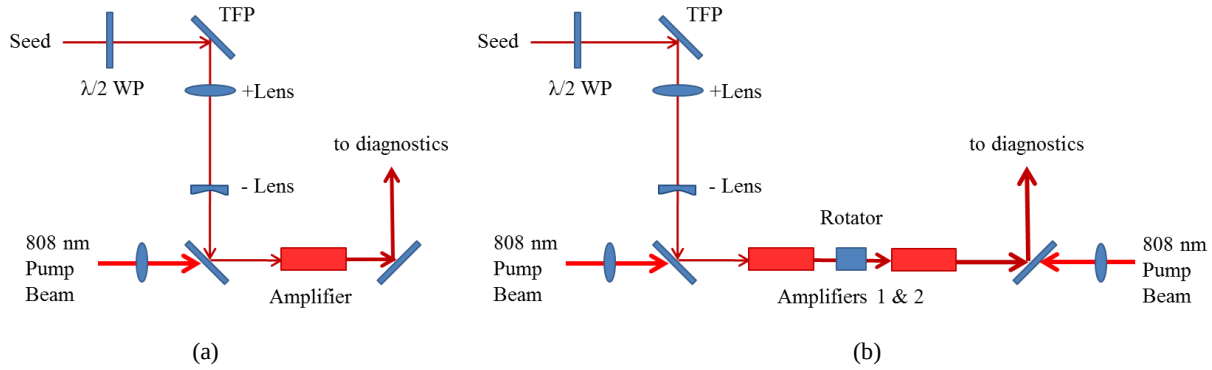

Figure 3: Schematic of amplifier testing set ups: (a) single amplifier testing set up is used to compare the performance of a single slab of each the standard and novel designs, and (b) two amplifiers of the novel design.

In all cases, the amplifier stage(s) consisted of an end pumped Nd:YAG slab mounted in a conductively cooled jacket (water flowed in the jacket but did not contact the slab). A 200 W fiber coupled 808 nm diode laser was used to pump each amplifier with 230 μs pulses at the same 500 Hz repetition rate as the oscillator.

Energy Scaling Results

In the single amplifier test set up, extraction efficiency of each style of amplifier was measured as a function of the seed energy received by the amplifier (Figure 4a). The maximum extraction efficiency of the new ceramic slab design was 24.6%, as compared to the efficiency of the old crystalline slab which was 20.6%. This constitutes a 19% increase in overall extraction efficiency between the two slab designs.

Using two of the novel ceramic slabs, a second amplification staged was aligned and the system was characterized in terms of beam quality and extraction efficiency. The energy extraction of the two amplifier set up is compared to that with a single amplifier of the same style (Figure 4b), showing a maximum extraction of 24.1% for the two amplifiers, which is comparable and within <1% of the single amplifier alone (24.6%).

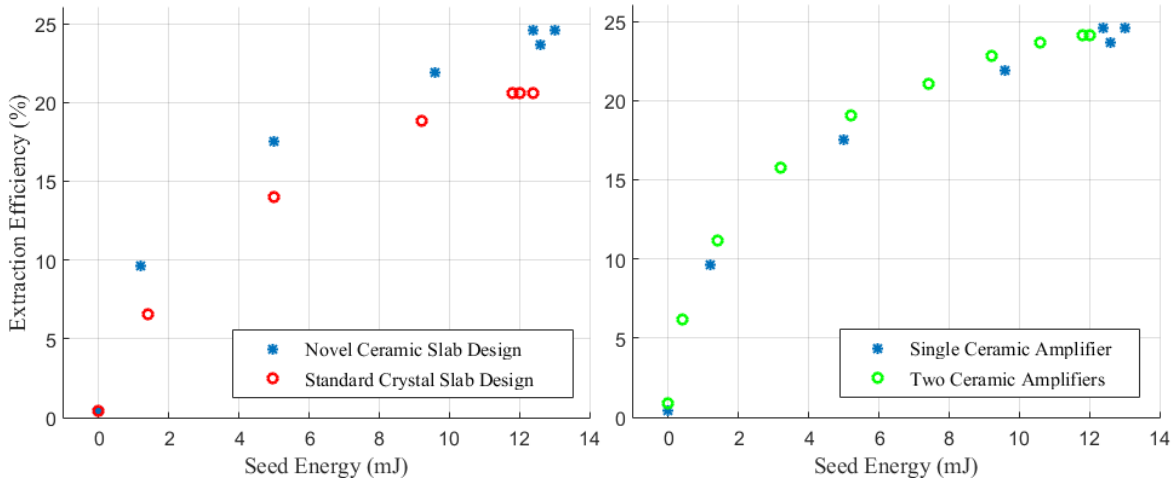

(a) (b)

Figure 4: a) comparison of extraction efficiency of a single standard slab vs. a novel slab; the novel design shows a 19% increase over previous designs, b) comparison of extraction behavior of one vs. two novel amplifier stages shows consistent performance

The far field image of the beam appears to be of the same character for all three cases examined, being both symmetrical and Gaussian (Figure 5).

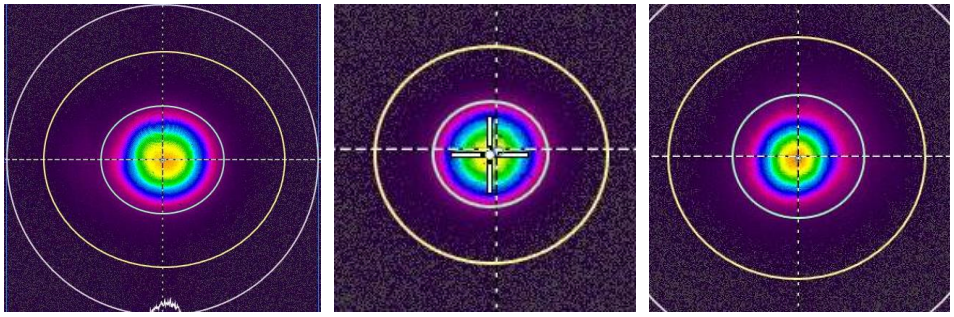

(a) (b) (c)

Figure 5: Far field beam images of a) a single stage of new amplifier design, b) a single stage of the standard amplifier design, and c) two stages of the new amplifier design.

The beam quality of the three cases was analyzed. Comparing the behavior for the two single-stage cases, a slightly higher M^2 value was observed for the new slab type (Table 1). The difference in M^2 between the two is most likely due to a slight change in the overlap between the pump beam and the seed beam as the new slab design is not expected to have an impact on the M^2 as compared with the previous design. Interestingly, the M^2 as measured with two amplifiers in place was reduced as compared with the single ceramic amplifier set up. This is because the ratio between the spot

size of the seed beam and the pump in the second amplifier was smaller than in the first amplifier. Because a substantial amount of energy was extracted from the second amplifier, this had a noticeable effect on the M^2.

Table 1: Comparison of M^2 values of new and standard slab designs

	M_x^2	M_y^2
Single Ceramic Amplifier	1.718	1.645
Single Standard Amplifier	1.557	1.458
Two Ceramic Amplifiers	1.557	1.458

The temporal width of the output pulses were examined before and after amplification. As is expected with an amplifier, the temporal width increased slightly. The pulses directly from the oscillator were 10.8 ns FWHM, and this increased to 12.5 and 12.8 ns with 1 and 2 stages of amplification respectively (Figure 6). Oscillator parameters can be adjusted as needed to achieve a specific pulse width (longer or shorter).

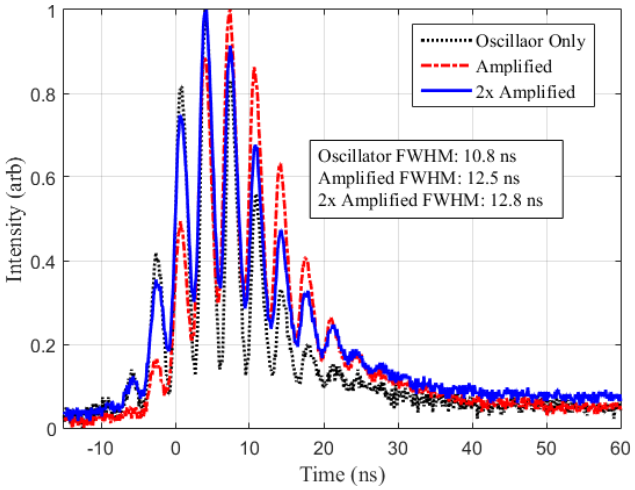

Figure 6: Temporal pulse width increases with amplification from 10.8 ns to 12.8 ns

3. NON-LINEAR CONVERSION EXPERIMENT

The second experiment demonstrates an efficient method of non-linear conversion (17%) to produce 452 nm light using 1064 nm pump pulses. Based on our experiments we estimate >20% conversion should be possible.

Non-linear Experimental Set Up

The second task was to efficiently convert 1064 nm light to blue light (452 nm). The methodology for generating blue light involves the use of three (3) nonlinear conversion stages (Figure 7). A 1064 nm pump laser operating at 50 Hz is used to pump a 4-mirror ring OPO with an intra-cavity frequency doubler. The OPO generates signal and idler at 1571 nm and 3.3 µm respectively, using a KTP crystal. The intra-cavity doubler, a BBO crystal, acts as the output coupler for the OPO by frequency doubling the 1571 nm light to produce 786 nm, which passes out of the cavity. This 786 nm light is redirected into an LBO Sum Frequency Mixing (SFM) crystal, where it is mixed with the original 1064 nm pump beam before it enters the OPO. The SFM crystal generates the blue output through the mixing of the 1064 nm and 786 nm pulses.

The OPO has several features of note. For the purpose of spectrally stabilizing the OPO output, a narrow 1571 nm DFB stabilized CW diode laser is coupled into the cavity through the 96% reflective output coupler (OC). This is important because the x-cut KTP crystal used in the cavity has the potential to generate spectral output with several nm of bandwidth; seeding narrows the spectral output and increases the conversion efficiency. The high reflectivity of the OC (96%) relates to the selection of the intra-cavity SHG crystal (as opposed to extra-cavity). By putting the SHG intra-cavity, it experiences a higher intensity of 1571 nm light than it would extra-cavity, increasing the overall conversion efficiency. By AR coating the OC at 786 nm, the SHG crystal therefore acts as a variable OC.

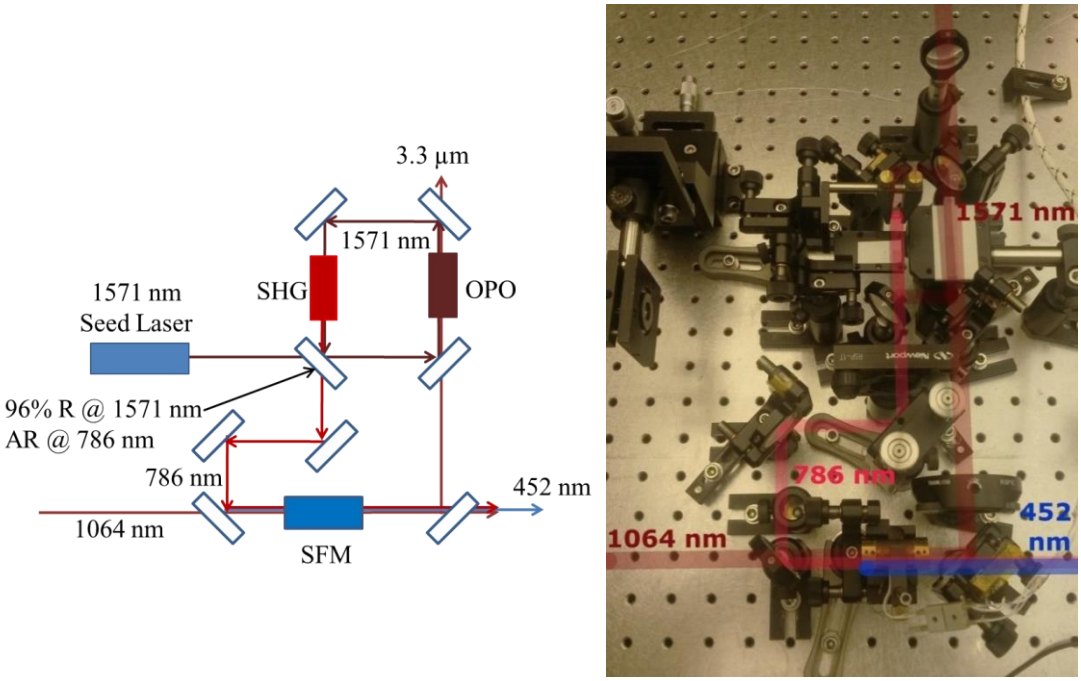

Figure 7: Schematic and photograph of the nonlinear conversion set-up

Non-linear Results

The nonlinear conversion system was assembled and output blue pulses (452 nm) with a maximum optical conversion efficiency of 17.1% from 1064 nm. The conversion efficiency increases linearly with the applied 1064 nm pump energy (Figure 8), with a maximum conversion efficiency of 17.1% at 18 mJ of pump energy. It should be noted that the applied pump energy was limited only by the damage threshold of the KTP crystal in the OPO. Greater conversion should be available at higher pump energies, and subsequent cavity designs and intra-cavity crystal selections can be made to ensure that damage thresholds do not remain a limiting factor.

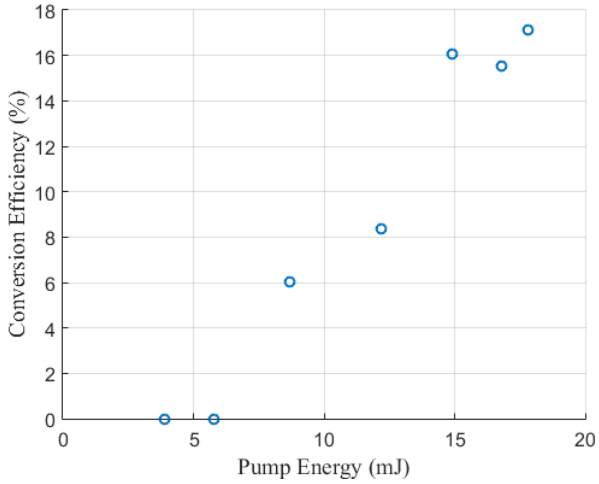

Figure 8: Conversion efficiency shown as a function of applied pump energy, and the maximum conversion efficiency from 1064 nm to 452 nm was17.1%.

As results were being collected for the 452 nm pulse energies, some hysteresis was noted as the 1064 nm pump power was increased and decreased. This behavior can be noted in the plot of the conversion efficiency, particularly the point at 15 mJ of pump energy. The likely cause of this behavior is heating of the KTP crystal in the OPO, which was not temperature stabilized in an oven. As the pump energy was increased and the crystal heated, the efficiency of the OPO

conversion likely increased, ultimately generating more blue light. Temperature stabilization and tuning of the KTP crystal by installing it in an oven should improve the performance of the OPO and enable a higher conversion to 452 nm.

The M^2 of the 452 nm beam and its profile were measured. The M^2 values for x and y were 1.245 and 1.651, respectively. The beam profile of the 452 nm beam is elliptical (Figure 9), resulting from a mismatch of the 786 and 1064 nm beams at the SFM crystal. The 1064 nm beam was conditioned using spherical and cylindrical lenses, but it was optimized for the location of the KTP crystal, and limited by the availability of lens curvatures on-hand. A better match of the 1064 and 786 nm beams at the SFM crystal would both increase conversion efficiency and the beam quality of the 452 nm beam.

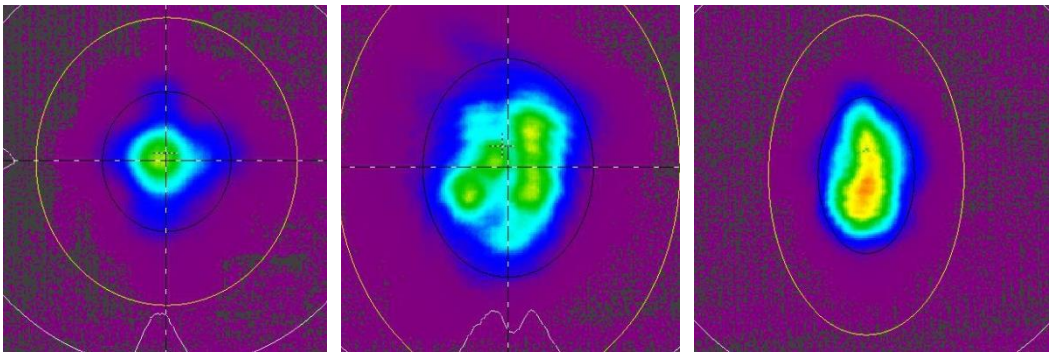

(a) (b) (c)

Figure 9: Beam profiles at SFM crystal a) 1064 nm, b) 786 nm, and c) 452 nm

A temporal offset between the 1064 nm pump pulse and the arrival of the 786 nm pulse was also observed (Figure 10), and if this offset could be reduced, an improvement in 452 nm conversion can also be expected. The temporal offset is 7 ns with the peak of the 786 nm pulse arriving after the peak of the 1064 nm pulse. This offset is primarily due to the OPO build up time, and secondarily with the physical layout of the system. This causes the 452 nm pulse to peak before the 786 nm pulse.

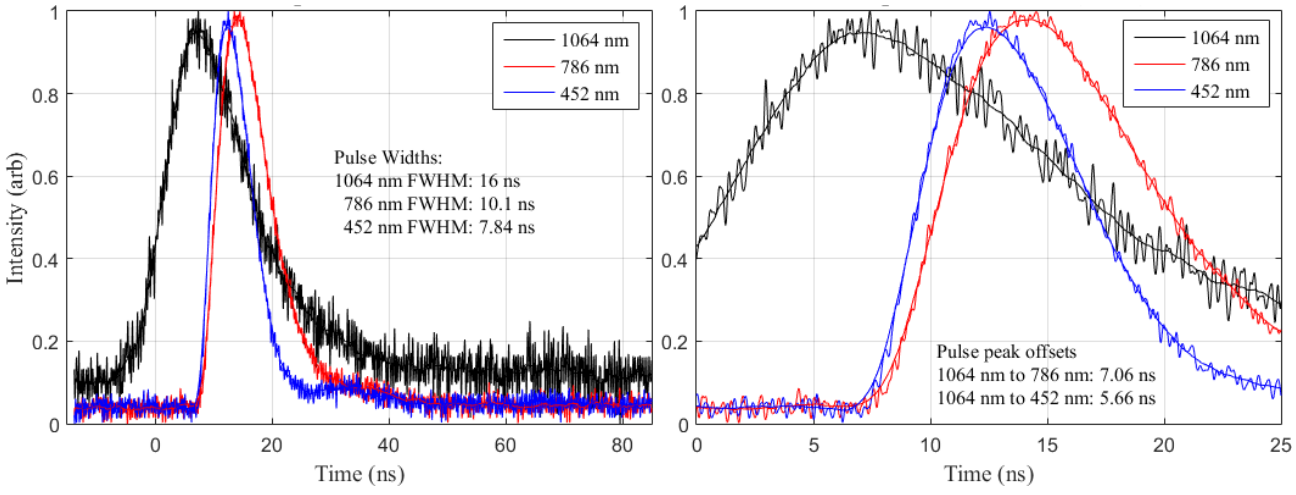

(a) (b)

Figure 10: a) temporal overlap of the pump (1064 nm), red (786 nm), and blue (452 nm) pulses, and b) inset

4. CONCLUSIONS

We demonstrate a multi-wavelength laser system for lidar-based applications. First we demonstrated an end pumped 1064 nm MOPA which employs novel progressively-doped ceramic Nd:YAG slab amplifiers, generating 34 mJ, 10.8 ns pulses at 500 Hz with a 24.6% extraction efficiency. A non-linear frequency-conversion system is also demonstrated, which consists of a ring OPO with an intra-cavity frequency-doubler. 1571 nm signal is generated which is doubled to

786 nm, and subsequently mixed with the 1064 nm pulses to generate 452 nm. The optical conversion efficiency of this process was 17.1%, generating 3 mJ of 452 nm pulses of 7.8 ns duration. Combining these two capabilities into a single high power, multi-line lidar system would constitute a significant advancement in the tools available for the study of atmospheric and oceanic ecosystems.

ACKNOWLEDGMENTS

Original research funded under the NASA Phase I SBIR contract "Laser Transmitter for Space-Based Atmospheric and Oceanographic Lidar".

REFERENCES

[1] N. G. Jerlov**,** Marine Optics, Elsevier Oceanography Series, New York, NY (1980).
[2] C. Czeranowsky, E. Heumann, and G. Huber, "All-solid-state continuous-wave frequency-doubled Nd:YAG–BiBO laser with 2.8-W output power at 473 nm," Opt. Lett. **28**, 432-434 (2003).
[3] Ole B. Jensen, and Paul M. Petersen, "A new approach to sum frequency generation of single-frequency blue light in a coupled ring cavity," Proc. SPIE 8964, Paper 896404 (2014);
[4] Felix Brunner, Edith Innerhofer, Sergio V. Marchese, Thomas Südmeyer, Rüdiger Paschotta, Takeshi Usami, Hiromasa Ito, Sunao Kurimura, Kenji Kitamura, Gunnar Arisholm, and Ursula Keller, "Powerful red-green-blue laser source pumped with a mode-locked thin disk laser," Opt. Lett. **29**, 1921-1923 (2004).
[5] Haibo Peng, Wei Hou, Yahui Chen, Dafu Cui, Zuyan Xu, Chuantian Chen, Feidie Fan, and Yong Zhu, "Generation of 7.6-W blue laser by frequency-tripling of a Nd:YAG laser in LBO crystals," Opt. Express **14**, 6543-6549 (2006).
[6] Zhu Haiyong, Zhang Ge, Huang Chenghui, Wei Yong, Huang Lingxiong, and Chen Zhenqiang, "Multi-watt power blue light generation by intracavity sum-frequency-mixing in $KTiOPO_4$ crystal," Opt. Express **16**, 2989-2994 (2008).